

Electrocatalytic Properties of Egg-white Sol-gel Derived $Mn_xFe_{3-x}O_4$ ($0 \leq x \leq 1.5$) for Alkaline Water Electrolysis

N.K. Singh^{*}, Ritu Yadav and M.K. Yadav

Department of Chemistry, Faculty of Science, University of Lucknow, Lucknow –226007 (India)

Received: September 21, 2016, Accepted: October 19, 2016, Available online: December 08, 2016

Abstract: Some binary ferrites having molecular formula, $Mn_xFe_{3-x}O_4$ ($0 \leq x \leq 1.5$) have been synthesized by a simple and cost effective egg white sol-gel route. In each preparation, nitrates of constituent metal were taken as starting materials and egg white as gelling agent. The material, thus obtained was altered in the form of film electrode on the pre-treated Ni- support using an oxide-slurry painting technique and investigated as electrocatalysts for the oxygen evolution reaction in KOH solutions. The study showed that Mn-substitution in the base oxide matrix influences the electrocatalytic activity of the material significantly and found to be greatest with 0.5 mol Mn-substitution. The reaction order has been found to be approximately unity with respect to OH^- concentration. The Tafel slope values at low potential ranged between ~ 52 and ~ 65 mVdecade⁻¹. The thermodynamic parameters namely, standard apparent electrochemical enthalpy of activation (ΔH_{a1}^{\ddagger}), standard enthalpy of activation (ΔH^{\ddagger}) and standard entropy of activation (ΔS^{\ddagger}) for the oxygen evolution reaction (OER) have also been determined. It has been observed that ΔH_{a1}^{\ddagger} and ΔH^{\ddagger} values decreased with Mn-substitution in the Fe_3O_4 lattice. This decrease in ΔH_{a1}^{\ddagger} and ΔH^{\ddagger} was found to be greatest with 0.5 mol Mn. The ΔS^{\ddagger} values were also found to be highly negative varying between ~ -185 and -211 J deg⁻¹ mol⁻¹.

Keywords: Egg white; sol-gel; Electrocatalysis; oxygen evolution, thermodynamic parameters

1. INTRODUCTION

Fossil fuels like coal, petroleum and natural gases are the main source of energy to meet the world's energy demand. However, these resources are unsustainable and depleting rapidly. Also, these fossil fuels primarily contribute to change the global climate by emitting noxious gases. These problems impelled researchers to develop clean and low cost energy solution by using various electrochemical devices like metals, alloys, metal oxides and transition metal mixed oxides with spinel and perovskite structure, in the form of electrocatalysts. The spinel-type oxide with general formula MM_2O_4 (where, M and M' are transition metal cations in +2 and +3 oxidation state, respectively) have long been known to constitute a wide class of electrode materials with good electrocatalytic activity for reactions such as O_2 evolution, Cl_2 evolution, O_2 reduction, H_2 formation and organic electrosynthesis [1]. These materials are most extensively studied and are widely used in high speed disk recording, electronic parts, magnetic fillers for rubber,

contrast enhancement of magnetic resonance imaging (MRI) and magnetically guided drug delivery [2-5]. It is reported in literature that ferros spinels have considerably higher overpotential for oxygen evolution [6] as compared to cobaltites [7-13]. However, it can be reduced by using low temperature preparation methods such as sol-gel, co-precipitation, hydrothermal etc and substituting suitable metal ion for Fe in the Fe_3O_4 matrix partially [14-25]. Mn-substituted spinel ferrites [16,19,20] are the best known versatile and reasonably soft ferromagnetic materials due to its mechanical hardness and chemical stability and showed a very good electrocatalytic properties towards oxygen evolution reaction (OER). Very recently, Maensiri et al. [26] used egg-white sol-gel route for the synthesis of spinel ferrites and studied their physical properties. It is reported in literature [27] that about 40 types of proteins are present in a chicken's egg-white. The egg-white is easily soluble in water and has a tendency to associate with metal ions in solution. Also, proteins of egg-white have various functional properties such as gelling, foaming, emulsification, heat setting and binding adhesion [27, 28]. Keeping the above facts in mind, we produced Mn-substituted ferrite materials by adopting the same

*To whom correspondence should be addressed:
Email: nksbhu@yahoo.com; singh_narendra@lkouniv.ac.in
Phone: +91-9451949105

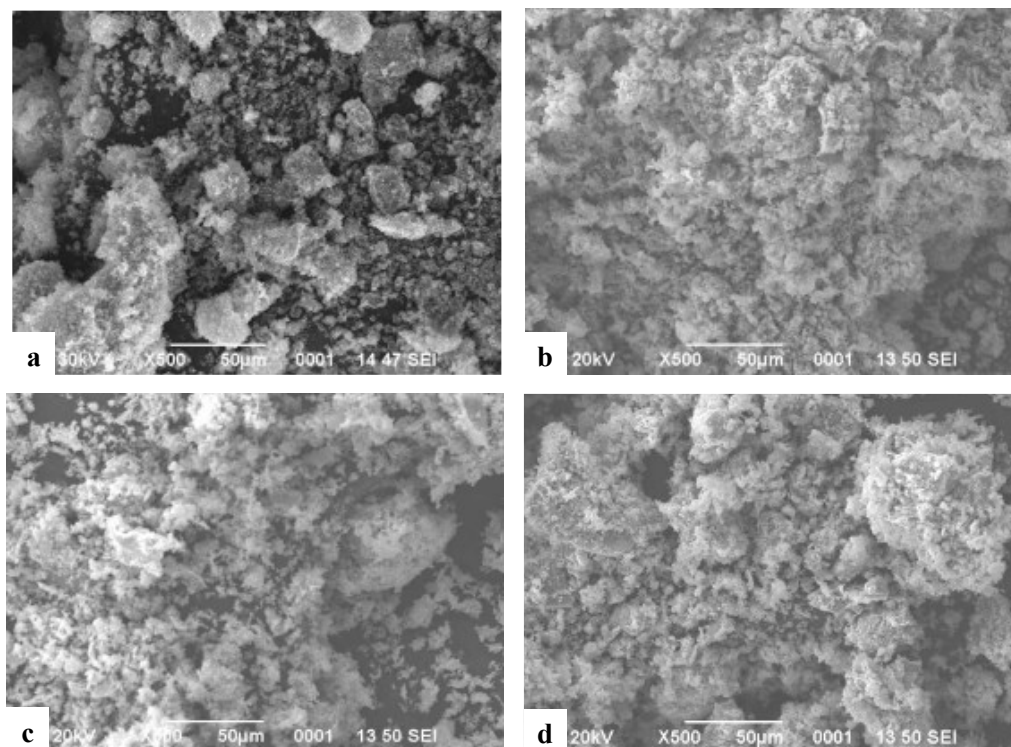


Figure 1. SE micrographs of oxide powders sintered at 500°C for 3 h at magnification ($\times 500$): (a) Fe_3O_4 , (b) $\text{Mn}_{0.5}\text{Fe}_{2.5}\text{O}_4$, (c) MnFe_2O_4 , (d) $\text{Mn}_{1.5}\text{Fe}_{1.5}\text{O}_4$

method reported Maensiri et al. [26] and studied their physico-chemical and electrocatalytic properties with regards to oxygen evolution in alkaline medium. The findings of results are described in this paper.

2. EXPERIMENTAL

Mn-substituted binary spinel oxides with composition $\text{Mn}_x\text{Fe}_{3-x}\text{O}_4$ ($0 \leq x \leq 1.5$), have been synthesized by simple egg-white sol-gel route [26]. For the purpose, purified $\text{Fe}(\text{NO}_3)_3 \cdot 9\text{H}_2\text{O}$ (Merck, 98%), $\text{Mn}(\text{NO}_3)_2 \cdot 4\text{H}_2\text{O}$ (Sigma-Aldrich, 97%) and freshly extracted egg-white (purchased from the local market) were taken as starting materials. As per stoichiometric ratio of the oxide, weighed amount of $\text{Fe}(\text{NO}_3)_3 \cdot 9\text{H}_2\text{O}$ and $\text{Mn}(\text{NO}_3)_2 \cdot 4\text{H}_2\text{O}$ were added in the homogeneous solution of egg-white (60 ml) and double distilled water (40 ml). The mixed solution was then evaporated on water bath at 80°C with constant stirring until a dried precursor was obtained. The dried precursor was crushed into powder and then sintered at 500°C for 3h to get the desired oxides. Powder X-ray diffraction pattern of materials was recorded with Bruker D-8 advanced series-2 diffractometer provided with $\text{Cu-K}\alpha_1$ as the radiation source (wave length $\lambda = 1.54056 \text{ \AA}$). Morphology of the oxide powder was determined by using scanning electron microscope (SEM; JEOL JSM 6490). Spinel ferrite phase of the material was confirmed by infrared spectra (FT-IR Thermoscientific; Nicole-6700).

In order to get the electrochemical investigations, oxide powders were transformed in the form of film electrode on a pre-treated Ni-support by an oxide slurry painting technique [29, 30]. The method of pre-treatment of Ni substrate, process of heat treatment in an

electrical furnace and electrical contact with the oxide film were adopted as described in the literature [29, 30].

All the electrochemical investigations that include cyclic voltammetry (CV) and anodic Tafel polarization were performed in a three electrode single compartment glass cell using potentiostat/galvanostat (Gamry Reference 600 ZRA) provided with corrosion and physical electrochemistry software and a desktop computer (HP). A platinum foil ($\sim 2\text{cm}^2$) and $\text{Hg}/\text{HgO}/1\text{M KOH}$ ($E^\circ = 0.098 \text{ V vs NHE at } 25^\circ\text{C}$) were used as an auxiliary and reference electrodes, respectively. The reference electrode was connected electrically to the electrolyte through a Luggin capillary (agar-agar and potassium chloride salt bridge gel) for the minimization of the solution resistance (iR drop) between the working and the reference electrode. The oxide film electrode was used as working electrode. The oxide film electrode was used as working electrode. The formal overpotential values mentioned in the data were obtained by the relation, $\eta = E - E_{\text{O}_2/\text{OH}^-}$, where E and $E_{\text{O}_2/\text{OH}^-}$ ($= 0.303 \text{ V vs. Hg}/\text{HgO}$) [31] are the applied potential across the catalyst/ 1 M KOH interface and the theoretical equilibrium Nernst potential in 1 M KOH at 25 °C, respectively.

3. RESULTS AND DISCUSSION

3.1. SEM, IR and XRD Studies

The SE-micrographs of pure and Mn-substituted oxide powder, sintered at 500 °C, are shown in Fig. 1 at the magnification X 500. Figure shows that Mn-substituted products have different morphological structure to that of base oxide. They exhibited more or less

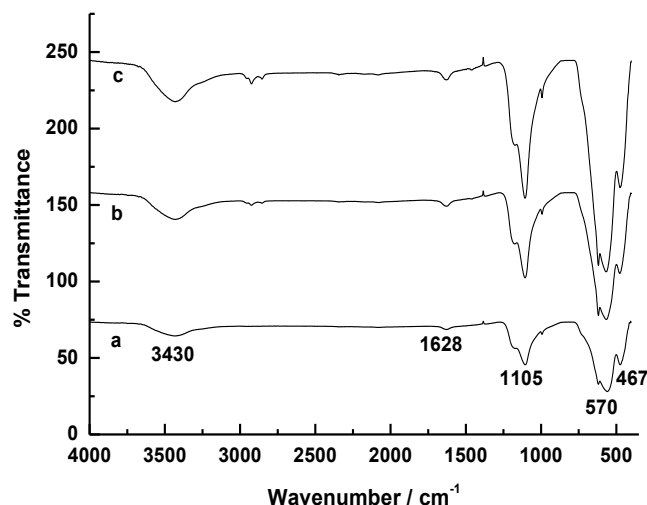


Figure 2. IR spectra of $Mn_xFe_{3-x}O_4$ ($x = 0.5, 1.0$ and 1.5) oxide sintered at 500°C for 3 h. (a) $Mn_{0.5}Fe_{2.5}O_4$, (b) $MnFe_2O_4$, (c) $Mn_{1.5}Fe_{1.5}O_4$

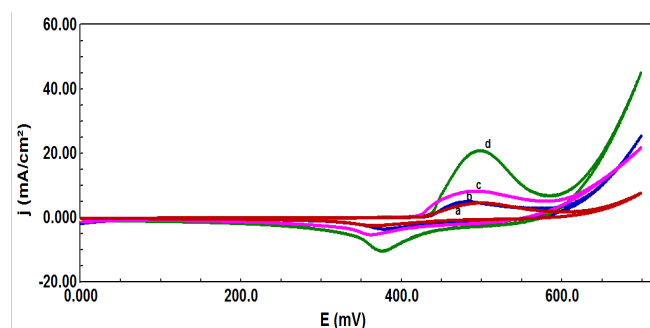


Figure 3. Cyclic Voltammograms of the oxide film electrodes on a Ni in 1 M KOH at 25°C (scan rate = 20 mV s^{-1}); Fe_3O_4 , (b) $Mn_{1.5}Fe_{1.5}O_4$, (c) $MnFe_2O_4$ and (d) $Mn_{0.5}Fe_{2.5}O_4$

cloudy structure. The distribution of particle is found to be more uniform and more homogeneous in the case of $Mn_{0.5}Fe_{2.5}O_4$.

IR spectra (Fig. 2) of $Mn_xFe_{3-x}O_4$ with $x = 0.5, 1.0$ and 1.5 , sintered at 500°C recorded in the region of $4000\text{--}400 \text{ cm}^{-1}$, exhibited a characteristic strong peak at $\sim 570 \text{ cm}^{-1}$ and $\sim 467 \text{ cm}^{-1}$ of pure spinel ferrite [32, 33]. The broad peak at $\sim 3430 \text{ cm}^{-1}$ observed in the Fig. 2 corresponds to the O-H stretching vibrations interacting through H-bonds.

The powder X-ray diffraction pattern of the material prepared was recorded between $2\theta = 20^\circ$ and 70° . The data obtained were analyzed by using JCPDS-ASTM file assuming cubic crystal geometry and found to best fit with JCPDS-ASTM file 10-0319 and 02-1035 for Fe_3O_4 and Mn-substituted ferrites, respectively. Some other additional diffraction peaks with d-values 1.45, 1.69, 1.84, 2.69 and 3.68 \AA (JCPDS-ASTM file 01-1053) observed in the patterns corresponds to the presence of Fe_2O_3 as impurities along with the spinel phase. The crystallite size was estimated by using the Scherrer formula [34] and found to be 44, 26, 32 and 34 nm for $x = 0, 0.5, 1.0$ and 1.5 , respectively.

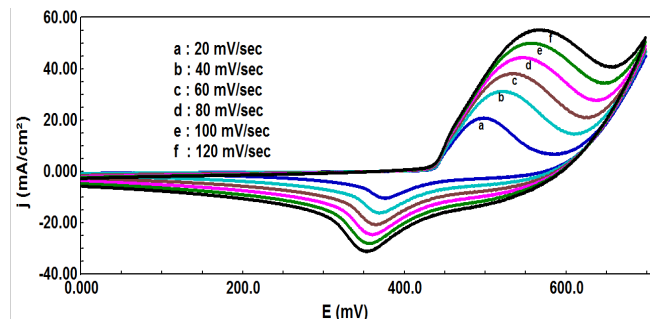


Figure 4. Cyclic voltammograms of $Ni/Mn_{0.5}Fe_{2.5}O_4$ electrode at different scan rates in 1 M KOH at 25°C .

3.2. Cyclic Voltammetry

Cyclic voltammograms of the catalytic film of pure and Mn-substituted ferrites on Ni support were recorded between $0.0\text{--}0.7 \text{ V}$ at scan rate of 20 mV sec^{-1} in 1 M KOH at 25°C . A representative curve of each oxide electrode is shown in Fig. 3. The figure 3 indicates that the observed voltammograms of the catalytic film on Ni were almost similar in nature regardless of the Mn-content in Fe_3O_4 lattice and showed a pair of redox peaks prior to the onset of oxygen evolution reaction (OER). Values of anodic (E_{pa}) and cathodic (E_{pc}) peak potentials, peak separation potential ($\Delta E = E_{pa} - E_{pc}$) and the formal redox potential [$E^\circ = (E_{pa} + E_{pc})/2$] for the surface redox reaction were estimated from the CV curve and are given in Table 1. The data shown in table 1 indicates that except 1.0 mol Mn-substitution, the value of ΔE_p was found to be almost same with each oxide catalyst. The decrease in the ΔE_p value with 1.0 mol Mn-substitution demonstrates a shift of surface redox processes towards reversibility. However, value of the formal redox potential (E°) was observed to be same with each oxide electrode. The observed values of formal redox potential were found to be similar to that originated due to the oxidation-reduction of bare Ni. This indicates that the redox peaks obtained with oxide film electrodes is originated from the Ni-support due to the contact with the electrolyte and not from the oxidation-reduction of oxide film. The electrolyte might reach to substrate (Ni-support) by hydration or through pores, cracks, intercrystalline gaps [8, 16, 30] formed in the catalytic film. However, this did not affect the stability of the catalytic over layer.

Cyclic voltammetric curves with each oxide electrode were also recorded at different scan rates (20 to 120 mV sec^{-1}) in 1 M KOH at 25°C . A representative CV curve for $Mn_{0.5}Fe_{2.5}O_4$ film electrode is shown in Fig. 4. Respective values of their E_{pa} , E_{pc} , ΔE_p , E° , i_{pa} , j_{pc} ,

Table 1. Values of the Cyclic Voltammetric parameters of $Ni/Mn_xFe_{3-x}O_4$ ($0 \leq x \leq 1.5$) in 1 M KOH at 25°C (scan rate = 20 mV sec^{-1})

Electrode	E_{pa} /mV	E_{pc} /mV	$\Delta E_p = (E_{pa} - E_{pc})$ /mV	$E^\circ = (E_{pa} + E_{pc})/2$ /mV
Fe_3O_4	505	362	143	434
$Mn_{0.5}Fe_{2.5}O_4$	497	375	122	436
$MnFe_2O_4$	493	362	103	430
$Mn_{1.5}Fe_{1.5}O_4$	481	378	131	428

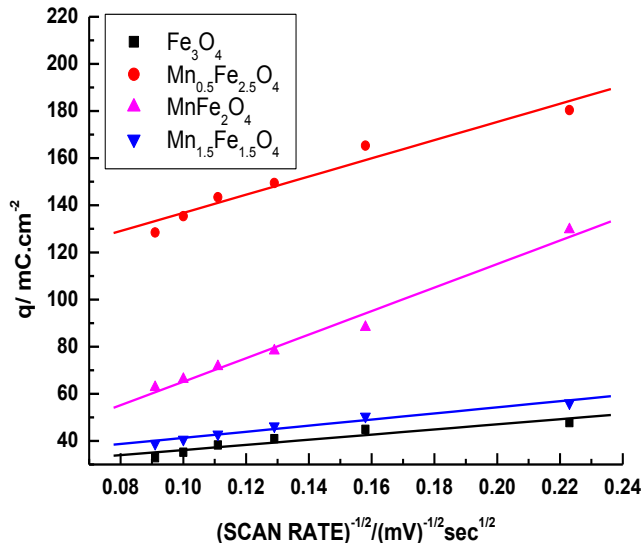


Figure 5. Plot of voltammetric charge (q) vs (scan rate) $^{-1/2}$ for oxide film electrode on Ni in 1 M KOH at 25°C.

j_{pa}/i_{pc} and q were determined from the CV curve and are listed in Table 2 (A & B). Data shown in Table 2 (A & B) indicates that with 6 fold increase in scan rate (20-120 mV sec^{-1}), the observed shift in the anodic and the cathodic peak potentials were found to be 52-105 mV and 16-32 mV towards higher potential and lower

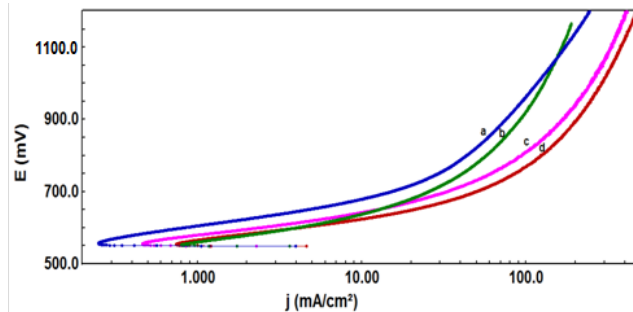


Figure 6. Tafel plots for oxygen evolution reaction on the Ni/Mn $_x$ Fe $_{3-x}$ O $_4$ ($0 \leq x \leq 1.5$) electrode in 1 M KOH at 25 °C (scan rate = 0.2 mV s^{-1}). (a) Fe $_3$ O $_4$ (b) MnFe $_2$ O $_4$, (c) Mn $_{1.5}$ Fe $_{1.5}$ O $_4$ and (d) Mn $_{0.5}$ Fe $_{2.5}$ O $_4$

potential side, respectively.

The voltammetric charge (q) is plotted as a function of (scan rate) $^{-1/2}$ with each oxide electrode and shown in the Fig. 5. The linearity observed in this plot indicates that the surface redox process is diffusion controlled.

3.3. Electrocatalytic activity

The electrocatalytic activity of pure and Mn-substituted ferrite film electrodes towards OER has been determined by recording the anodic polarization curve in 1 M KOH at 25 °C. A representative figure is shown in Fig. 6. From figure 6, it has been observed that

Table 2 (A). Cyclic Voltammetric parameters for the Mn $_x$ Fe $_{3-x}$ O $_4$ ($x = 0$ and 0.5) film on Ni in 1 M KOH at 25 °C.

Scan rate / mVsec^{-1}	E_{pa} /mV	E_{pc} /mV	$\Delta E_p = (E_{pa} - E_{pc})$ / mV	$E^\circ = (E_{pa} + E_{pc})/2$ / mV	j_{pa} /mA cm^{-2}	j_{pc} /mA cm^{-2}	$ j_{pa} / j_{pc} $	q /mC cm^{-2}
20	505	362	143	434	4.6	2.5	1.8	47.8
	(497)	(375)	(122)	(436)	(20.9)	(10.4)	(2.0)	(180.4)
40	529	361	168	445	7.0	3.9	1.8	44.9
	(522)	(369)	(153)	(445)	(31.3)	(16.2)	(1.9)	(165.3)
60	549	354	195	451	8.8	5.1	1.7	41.1
	(535)	(364)	(171)	(449)	(38.3)	(20.8)	(1.8)	(149.5)
80	573	354	219	464	10.6	6.1	1.7	38.3
	(546)	(360)	(186)	(453)	(44.5)	(24.6)	(1.8)	(143.4)
100	578	351	227	465	11.8	6.9	1.7	35.2
	(555)	(356)	(199)	(456)	(50.1)	(28.1)	(1.8)	(135.4)
120	600	347	253	474	13.4	5.6	1.7	32.9
	(565)	(352)	(213)	(458)	(55.4)	(31.2)	(1.8)	(128.5)

(Note: The values written in parenthesis correspond to Mn $_{0.5}$ Fe $_{2.5}$ O $_4$ electrode.)

Table 2 (B). Cyclic Voltammetric parameters for the Mn $_x$ Fe $_{3-x}$ O $_4$ ($x = 1$ and 1.5) film on Ni in 1 M KOH at 25°C.

Scan rate / mVsec^{-1}	E_{pa} /mV	E_{pc} /mV	$\Delta E_p = (E_{pa} - E_{pc})$ /mV	$E^\circ = (E_{pa} + E_{pc})/2$ / mV	j_{pa} /mA cm^{-2}	j_{pc} /mA cm^{-2}	$ j_{pa} / j_{pc} $	q /mC cm^{-2}
20	481	378	103	430	5.0	3.5	1.4	129.7
	(493)	(362)	(131)	(428)	(8.3)	(5.3)	(1.6)	(56.1)
40	506	373	133	440	8.4	5.8	1.4	88.3
	(534)	(352)	(182)	(443)	(13.5)	(8.4)	(1.6)	(50.4)
60	517	367	150	442	10.9	7.6	1.4	78.7
	(561)	(346)	(215)	(454)	(16.6)	(10.8)	(1.5)	(46.3)
80	523	367	156	445	13.2	9.2	1.4	71.6
	(571)	(338)	(233)	(455)	(19.6)	(12.9)	(1.5)	(42.9)
100	529	364	165	447	14.9	10.6	1.4	66.2
	(580)	(333)	(247)	(457)	(22.2)	(14.7)	(1.5)	(40.7)
120	533	362	171	448	16.9	11.8	1.4	62.7
	(598)	(330)	(268)	(464)	(24.6)	(16.3)	(1.5)	(38.9)

(Note: The values written in parenthesis correspond to Mn $_{1.5}$ Fe $_{1.5}$ O $_4$ electrode.)

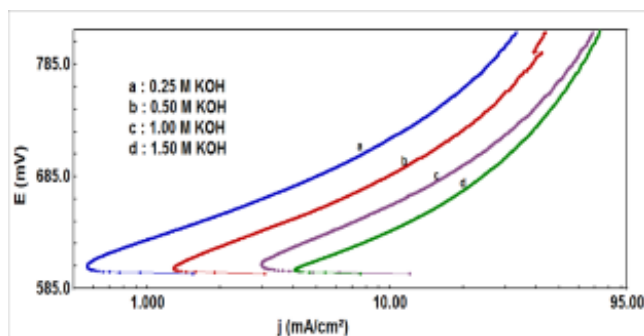


Figure 7. Tafel plots for oxygen evolution on Ni/MnFe₂O₄ electrode at varying KOH concentrations ($m = 1.5$) at 25 °C.

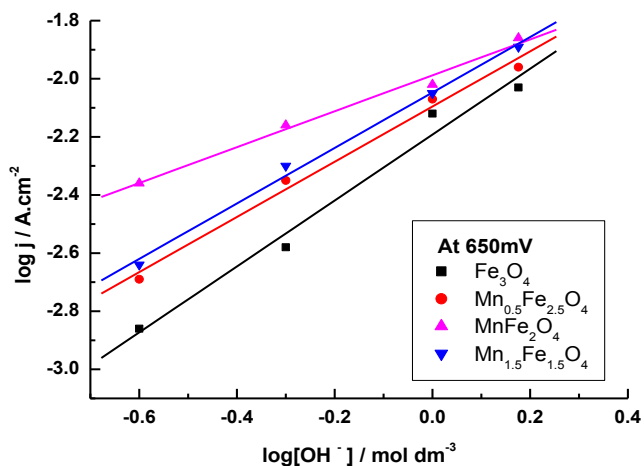


Figure 8. Plot of $\log j$ vs $\log [OH^-]$ of oxide electrodes at a constant potential ($E = 650$ mV) at 25 °C.

each polarization curve showed one well defined slope up to the current density 50–100 mA cm⁻² and it progressively increased thereafter. The Mn-substitution in the base oxide showed marginal reduction of Tafel slope for the oxygen evolution reaction and ranged between 52 and 65 mV decade⁻¹. The magnitude of reduction being maximum with 0.5 mol Mn-substitution in the base oxide. Values of Tafel slope (b) and the electrocatalytic activity in terms of current density at three different overpotentials as well as in terms of overpotential at fixed current density were estimated from the polarization curve and given in Table 3.

Data shown in the table 3 indicates that Mn-substitution in the Fe₃O₄ lattice lowers the oxygen overpotential and being found to be maximum with 0.5 mol Mn. At the apparent current density of 100

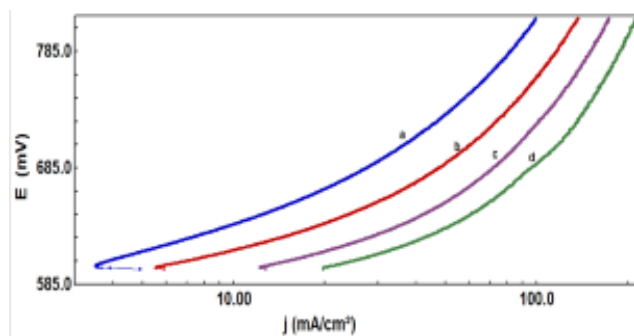


Figure 9. Tafel plots for Ni/Mn_{0.5}Fe_{2.5}O₄ electrode in 1 M KOH at different temperatures (scan rate = 0.2 mV s⁻¹), (a) 20 °C, (b) 30 °C, (c) 40 °C and (d) 50 °C

mA cm⁻², 0.5 mol Mn-substitution decreased the overpotential value by ~ 200 mV. Based on the current density data at certain overpotential (= 547 mV), the electrocatalytic activity of oxides followed the order:

Mn_{0.5}Fe_{2.5}O₄ ($j_a = 171.4$ mA cm⁻²) > Mn_{1.5}Fe_{1.5}O₄ ($j_a = 133.0$ mA cm⁻²) > MnFe₂O₄ ($j_a = 75.2$ mA cm⁻²) > Fe₃O₄ ($j_a = 59.6$ mA cm⁻²).

To determine the order of reaction, the polarization curves for each oxide electrode were recorded in different KOH concentrations (0.25–1.5 M) by keeping the ionic strength ($\mu = 1.5$) constant by adding suitable amount of KNO₃ (an inert electrolyte). Fig. 7 shows the polarization curves for Mn_{0.5}Fe_{2.5}O₄ recorded in different KOH concentrations. The value of reaction order (p) with each oxide electrode was estimated from the slope of the plot $\log j$ vs $\log [OH^-]$ [Fig. 8] at a certain potential ($E = 650$ mV) across the oxide film / KOH solution interface. For the determination of reaction order, first linear region of Tafel polarization curves were chosen in each case. The estimated values of reaction order (p) for each catalyst are given in Table 3.

The observed p and b-value with each oxide electrode was found to be close to 2.3RT/F which suggests that the OER on pure and Mn-substituted ferrite follow almost similar mechanistic paths. It is noteworthy that the Mn-substituted oxide electrodes prepared by us were more active than those of other ferrite electrodes already reported in literature [15, 22–25, 35–37]. Iwakura et al [35, 36] (at $j_a = 10$ mA cm⁻²) observed $\eta_{O_2} = 440$ and 580 mV on CoFe₂O₄ and MnFe₂O₄, respectively in 1 M KOH at 25°C. Orehtsky et al [37] found $\eta_{O_2} = 340$ mV on NiFe₂O₄ in 30 wt % KOH. On the other hand, electrodes, Mn_{0.5}Fe_{2.5}O₄, MnFe₂O₄ and Mn_{1.5}Fe_{1.5}O₄ prepared by us in the present series produced significantly low $\eta_{O_2} = 317, 327, 339$ mV, respectively, in 1 M KOH at 25°C at $j_a = 10$ mA cm⁻². Al-Mayouf et al [22] observed $j_a = 0.62$ mA cm⁻² at $E = 0.650$ V

Table 3. Electrode kinetic parameters for oxygen evolution reaction on pure and Ni-substituted ferrite electrodes in 1 M KOH at 25 °C

Electrode	Tafel slope /mVd ⁻¹	Order (p)	η_{O_2} /mV at j (mA cm ⁻²)			j (mA cm ⁻²) at η_{O_2} /mV		
			10	100	200	347	447	547
Fe ₃ O ₄	65	1.1	374	660	833	4.9	29.8	59.6
Mn _{0.5} Fe _{2.5} O ₄	52	0.9	317	462	583	21.3	87.1	171.4
MnFe ₂ O ₄	62	0.9	327	614	780	13.5	41.3	75.2
Mn _{1.5} Fe _{1.5} O ₄	54	0.8	339	500	635	13.6	64.0	133.0

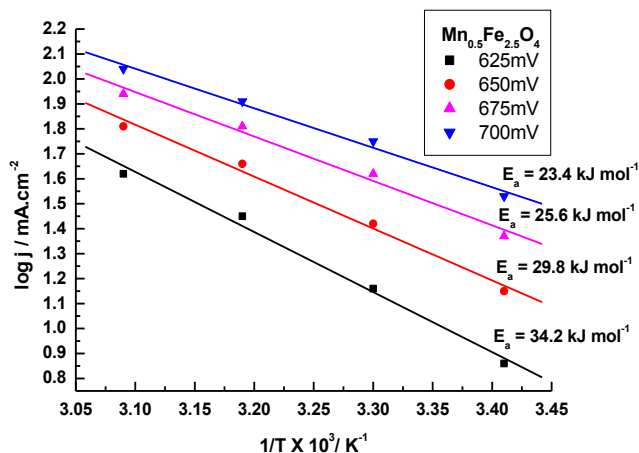


Figure 10. Arrhenius plot for oxygen evolution reaction on Ni/Mn_{0.5}Fe_{1.5}O₄ at different potential.

in 1 M KOH at 25°C for NiFe₂O₄ whereas Mn_{0.5}Fe_{2.5}O₄ prepared by us showed $j_a = 21.3 \text{ mA cm}^{-2}$ at the same potential under the similar experimental conditions.

The activation energy of oxide electrodes were determined by recording the anodic polarization curves in 1 M KOH at different temperatures (20°-50°C). A representative polarization curves for Mn_{0.5}Fe_{2.5}O₄ film electrode at different temperatures in 1 M KOH is shown in Fig. 9. With the help of polarization curves, Arrhenius plot (i.e. $\log j$ vs. $1/T$), was constructed at different constant potentials as shown in Fig. 10 for Mn_{0.5}Fe_{1.5}O₄ film electrode. Figure shows that the value of activation is decreased as the potential is increased. The value of activation energy ($\Delta H_{ei}^{\circ\ddagger}$) was estimated from the slope of straight line and found to be 45.9, 34.2, 42.7 and 40.6 kJ mol⁻¹ for Fe₃O₄, Mn_{0.5}Fe_{2.5}O₄, MnFe₂O₄ and Mn_{1.5}Fe_{1.5}O₄, respectively at $E = 625 \text{ mV}$. With the help of $\Delta H_{ei}^{\circ\ddagger}$ values, $\Delta H^{\circ\ddagger}$ values were calculated by using relation, $\Delta H_{ei}^{\circ\ddagger} = \Delta H^{\circ\ddagger} - \alpha F\eta$, where, $\Delta H^{\circ\ddagger}$ is the standard enthalpy of activation ($= \Delta H_{ei}^{\circ\ddagger}$ at $\eta = 0$ or $E = E_{rev}$) and $\alpha F\eta$ is the electrical contribution. The transfer coefficient (α) was estimated by using the equation $\alpha = 2.303RT/bF$, where, b is the Tafel slope in mVdecade⁻¹, T is absolute temperature, R and F are the gas constant and Faraday constant, respectively. The Tafel slope (b) value is calculated from the slope of the polarization curves obtained at different temperatures. The standard entropy of activation ($\Delta S^{\circ\ddagger}$) for oxygen evolution was estimated using the relation given in literature [38].

Table 4. Thermodynamic parameters for O₂ evolution on Ni / Mn_xFe_{3-x}O₄ (0 ≤ x ≤ 1.5) in 1M KOH

Electrode	$\Delta H_{ei}^{\circ\ddagger}$ (kJ mol ⁻¹) at $E = 625 \text{ mV}$	$\Delta S^{\circ\ddagger}$ (J deg ⁻¹ mol ⁻¹)	α	$\Delta H^{\circ\ddagger}$ (kJ mol ⁻¹)
Fe ₃ O ₄	45.9	185.5	0.9	63.5
Mn _{0.5} Fe _{2.5} O ₄	34.2	211.5	1.1	66.4
MnFe ₂ O ₄	42.7	185.1	1.0	63.9
Mn _{1.5} Fe _{1.5} O ₄	40.6	194.4	1.1	64.9

$$\Delta S^{\circ\ddagger} = 2.3R \left[\log j + \frac{\Delta H_{ei}^{\circ\ddagger}}{2.3RT} - \log(nF\omega C_{OH^-}) \right]$$

Where $\omega (= k_B T/h)$ is the frequency term and $n = 2$ and all other terms used in the above equation have their usual meanings. The estimated values of α , $\Delta H_{ei}^{\circ\ddagger}$, $\Delta H^{\circ\ddagger}$ and $\Delta S^{\circ\ddagger}$ are given in Table 4. Values of $\Delta H_{ei}^{\circ\ddagger}$ for OER on different catalysts in 1 M KOH ranged between 34.2 and 45.9 kJ mol⁻¹ at $E = 625 \text{ mV}$. The observed $\Delta H_{ei}^{\circ\ddagger}$ value for OE was almost similar to that reported on Adams-RuO₂ (49 kJ mol⁻¹) [39], oxide coated Co₅₀Ni₂₅B₁₀ amorphous alloy (40 kJ mol⁻¹) [40] and Cu_{0.9}Co_{2.1}O₄ (45.2 kJ mol⁻¹) [41].

4. CONCLUSION

The above study indicates that the partial substitution of Mn for Fe in the Fe₃O₄ lattice enhances the apparent electrocatalytic activity of the oxide and it was found to be maximum with 0.5 mol Mn-substitution. Thus, the requisite level of Mn-substitution into the Fe₃O₄ lattice influenced the geometrical as well as the electrocatalytic properties of oxides favourably.

5. ACKNOWLEDGEMENTS

Authors are thankful to Dr Jhasaketan, Department of Chemistry, IIT Kanpur, Kanpur for carrying XRD analysis. They are also grateful to Department of Science and Technology (DST), New Delhi for financial support as Fast Track Scheme for Young Scientist (No.: SR/FT/CS-044/2009).

REFERENCES

- Trasatti S., Transition metal oxides: versatile materials for electrolysis, In: Lipkowski J, Ross PN, editors. The electrochemistry of novel materials. Weinheim: VCH Publishers; p-207 (1994).
- Bueno Alexandre R., Gregori Maria L., Nobrega Maria C. S., J. Magn Magn Mater, 320, 864 (2008).
- Arias Jose L., Ruiz Adolfin M., Gallardo Visitacion, J. Controlled Release, 125(1), 50 (2008).
- Zhang Yan-Qing, Zhang Xiong, J. Inorganic Materials, 21(4), 861 (2006).
- Mitchell D. G., J. Magn Reson Imaging, 7, 1 (1997).
- Allen P.D., Hampson N.A., Bignold G.J., J. Electroanal. Chem., 99, 299 (1979).
- O'Sullivan E.J.M., Calvo E.J., Comprehensive chemical kinetics, Amsterdam: Elsevier; 27, 263 (1987).
- Trasatti S., In: Lipkowski J, Ross PN., Electrochemistry of novel materials, New York: VCH; pp. 207 (1994).
- Tavares A.C., Bochatay L., Da Silva Pereira M.I., Da Costa F.M.A., Electrochim Acta, 41, 1953 (1996).
- Tavares A.C., Cartaxo M.A.M., Da Silva Pereira M.I., Da Costa F.M.A., J. SolidState Chem., 5, 57 (2001).
- Tavares A.C., Cartaxo M.A.M., Da Silva Pereira M.I., Da Costa F.M.A., J. Electroanal. Chem., 464, 187 (1999).
- Rios E., Gautier J-L, Poillierat G., Chartier P., Electrochim. Acta, 44, 1491 (1998).
- Svegl F., Orel B., Grabec-Svegl I., Kaucic V., Electrochim. Acta, 45, 4359 (2000).

- [14]Singh R.N., Singh N.K., Singh J.P., *Electrochim. Acta*, 47, 3873 (2002).
- [15]Singh J.P., Singh N.K., Singh R.N., *Int. J. Hydrogen Energy*, 24, 433 (1999).
- [16]Singh N.K., Tiwari S.K., Anitha K.L., Singh R.N., *J. Chem. Soc. Faraday Trans*, 92(14), 2397 (1996).
- [17]Singh N.K., Singh R.N., *Ind. J. Chem.*, 38A, 491 (1999).
- [18]Singh R.N., Singh J.P., Lal B., Thomas M.J.K., Bera S., *Electrochim. Acta*, 51, 5515 (2006).
- [19]Singh R.N., Singh J.P., Cong Nguyen H., Chartier P., *Int. J. Hydrogen energy*, 31, 1372 (2006).
- [20]Singh R.N., Singh J.P., Cong Nguyen H., Chartier P., *Int. J. Hydrogen Energy*, 31, 1372 (2006).
- [21]Singh R. N., Singh J. P., Lal B., Singh A., *Int. J. Hydrogen Energy*, 32, 11 (2007).
- [22]Al-Hoshan M.S., Singh J.P., Al-Mayouf A.M., Al-Suhybani A. A., Shaddad M.N., *Int. J. Electrochem. Sci.*, 7, 4959 (2012).
- [23]Yadav Ritu, Yadav M.K., Singh N.K., *Int. J. Electrochem. Sci.*, 8, 6321 (2013).
- [24]Yadav Ritu, Singh N.K., *Ind. J. Chem.*, 54A, 1221 (2015).
- [25]Yadav Ritu, Jhasaketan, Singh N.K., *Int. J. Electrochem. Sci.*, 10, 9297 (2015).
- [26]Santi Maensiri, Chivalrat Masingboon, Banjong Boonchomb, *Scripta Materialia*, 56, 797 (2007).
- [27]Lu R., Yang D., Cui D., Wang Z., Guo L., *Int. J. Nanomedicine*, 7, 2101 (2012).
- [28]Mine Y., *J. Worlds Poult Sci.*, 58, 31 (2002).
- [29]Singh R.N., Tiwari S.K., Singh S.P., Singh N.K., Poillerat G., Chartier P., *J.Chem. Soc. Faraday Trans.*, 92(14), 2593 (1996).
- [30]Tiwari S.K., Chartier P., Singh R.N., *J. Electrochem. Soc.*, 142, 148 (1995).
- [31]Singh R.N., Pandey J.P., Singh N.K., Lal B., Chartier P., Koenig J. F., *Electrochim Acta*, 45, 1911 (2000).
- [32]Okasha N., *Mater. Chem. Phys.*, 84, 63 (2004).
- [33]Gillot B., Nivoix V., Kester E., Nusillard O., Villette C., Tailhades Ph., Rousset A., *Mater. Chem. Phys.*, 48, 111 (1997).
- [34]Fradette N., Marsan B., *J. Electrochem. Soc.*, 145(7), 2320 (1998).
- [35]Iwakura C., Nishioka M., Tamura H., *Nippon Kagaku Kashi*, 7, 1136 (1982).
- [36]Iwakura C., Nishioka M., Tamura H., *Denki Kagaku*, 49, 355 (1981).
- [37]Orehotsky J., Huang H., Davidson C.R., Srinivasan S., *J. Electroanal. Chem.* 95, 233 (1979).
- [38]Gileadi E., *Electrode Kinetics*, VCH Publishers Inc. New York, p. 151 (1993).
- [39]Mills A., Davis H.L., *Electrochim. Acta*, 37(7), 1217 (1992).
- [40]Kessler T., Triaca W.E., Arvia A.J., *J. Appl. Electrochem.*, 24, 310 (1994).
- [41]Nikolov I., Darkaou R., Zhecheva E., Stoyanova R., Dimitrov N., Vitanov T., *J. Electroanal. Chem.*, 429, 157 (1997).